# Deterioration of Depth Measurements Due to Interference of Multiple RGB-D Sensors

Roberto Martín Martín[1] Malte Lorbach[1] Oliver Brock[1]

***Abstract*— Depth sensors based on projected structured light have become standard in robotics research. However, when several of these sensors share the same workspace, the measurement quality can deteriorate significantly due to interference of the projected light patterns. We present a comprehensive study of this effect in Kinect and Xtion RGB-D sensors. In particular, our study investigates the effect of measurement failure due to interference. Our experiments show that up to 95% of the depth measurements in the interference image region can disappear when two RGB-D sensors interfere with each other. We determine the severity of interference as a function of relative sensor placement and propose simple guidelines to reduce the impact of sensor interference. We show that these guidelines greatly increase the robustness of RGB-D-based SLAM.**

## I. Introduction

Depth sensors based on projected structured light have become prevalent in robotics. In 2013, well over 10 percent of papers published in the main robotics venues included the Kinect or similar RGB-D sensors, such as the Asus Xtion.[2] Depth sensors are affordable, accurate, and provide reliable depth data at high resolution and frame rate. However, they also have a significant drawback. As with any type of active sensor, the measurements of two depth sensors may interfere with each other. When their projected light patterns overlap or one camera projects its pattern directly into the sensor of the other camera, measurement quality can deteriorate. This effect has been recognized as significant in a few cases [1, 2, 3], however, nobody has ever analyzed completely the correlation of the interference to the relative sensor pose.

The objective of this paper is to provide a thorough analysis of the effects of interference between commercially available RGB-D sensors based on projected structured light. Our analysis is intended as a guide for experimental design and to inform the design of future generations of RGB-D sensors. We used more than 260,000 depth maps to evaluate the effect of sensor interference. These experiments focused on three scenarios: two sensors looking at the same point in space from different positions, two sensors with parallel viewing directions, and two sensors facing each other (Fig. 1). Moreover, we demonstrate that our characterization can be used to improve a real RGB-D-based application: simultaneous localization and mapping (SLAM) based on iterative closest points (ICP).

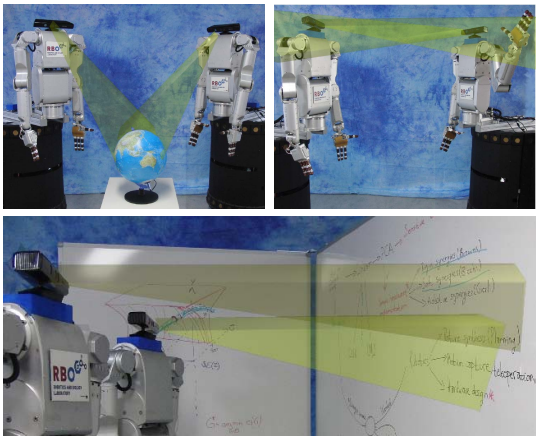

Fig. 1. Interference between two RGB-D sensors causes depth measurement failure: two robots looking at the same scene with intersecting viewing directions, opposite viewing directions, and parallel viewing directions.

Our experiments show that sensor interference can cause measurement failure in up to 95% of the pixels in the interference region. The percentage varies significantly based on the relative position and orientation of the sensors. There are extensive regions in the space of relative poses for two sensors in which interference is limited; these regions should be preferred in experiments with multiple sensors. Our experiments also show that the overall measurement accuracy and precision remain largely unaffected by the interference in those cases in which depth measurements can be obtained. The results constitute conclusive evidence that measurement interference is a significant problem in existing RGB-D sensors based on projected structured light. The effect of interference must be considered in experimental setups in which multiple robots operate in the same workspace.

## II. Structured-Light Depth Sensors

All structured light depth sensors share the same working principle: they project a known light pattern into the environment and observe the distortion caused by surfaces. The distortion, together with triangulation, provide depth and shape information about the scene. To perform triangulation, it is necessary to match projected light patches with the undistorted projected pattern. Many designs following this principle have been proposed. Some devices use a striped, colored light pattern [4]. Color is easily identified but the sensor can only measure depth of texture-less/color-less

We gratefully acknowledge the funding provided by the Alexander von Humboldt foundation and the Federal Ministry of Education and Research (BMBF) and through the First-MM project (European Commission,FP7-ICT-248258). We thank SimLab for their support.

[1]Robotics and Biology Laboratory, Technische Universität Berlin

[2]ICRA 2013: 12%, IROS 2013: 15%, RSS 2013: 24%, IJRR 2013: 6%. Results of searching for words: *Kinect*, *Asus*, *PrimeSense*, *Xtion*, *RGB-D*.


Fig. 2. RGB-D sensor Kinect (left): an infrared pattern (right) is projected into the scene; the depth information obtained from infrared measurements is combined with the RGB image to yield an RGB-D image

surfaces. Proesmans et al. [5] project a grid and assume continuity of the surface in the environment. Due to this limiting assumption, this sensor fails on discontinuous surfaces. Other authors use light patterns that vary over time [6]. These sensors start projecting few stripes and divide each stripe in the next time step. The coarse-to-fine methodology simplifies the light pattern recognition but increases acquisition time, and thus cannot be used in dynamic environments.

The company PrimeSense overcame the challenge of matching an observed surface patch to a part of the projected pattern by projecting a pattern consisting of $211 \times 165$ infrared speckles [7, 8]. This pattern is repeated in a $3 \times 3$ grid to form the sensor's overall projection pattern. A high resolution IR camera (Fig. 2) captures the projected pattern that is processed to estimate a depth map. This depth map is combined with an RGB-sensor to yield the resulting RGB-D image. Three frequently used sensors following this principle are Microsoft Kinect, Asus Xtion series and PrimeSense Carmine series. Based on our evaluation, these three sensors contain the identical hardware. In our experiments, we use the Kinect and the Asus Xtion interchangeably and obtain identical results.

In November 2013 Microsoft released the Kinect 2. The technology for the depth estimation changes from infrared projected light to time of flight (ToF), another type of active sensing which also suffers of degradation due to interference. As soon as it becomes available for robotic applications, a similar interference analysis should be carried out.

## III. Related Work

### A. Studies of Sensor Quality

Several authors analyzed measurement quality of single RGB-D sensors. Andersen [9] performed an evaluation of the accuracy and precision of the sensor in the context of computer vision applications. He detected measurement degradation (higher probability of measurement failure) due to interference but does not explore this effect. Viager [10] reports that sensor interference most often causes measurement failures and only rarely leads to reduction in measurement accuracy or precision. He concludes that an in-depth study of sensor interference is required.

These studies focused on sensor accuracy (mean error between the measured depth value and the ground truth at each pixel) and precision (standard deviation of the error). However, there is a third failure mode: RGB-D sensors may fail to estimate the depth on a location. Berger et al. [1] observed this effect when they developed a motion capture system based on multiple Kinect cameras. They report that the probability of measurement failure increases with the number of Kinects, narrower angles between the viewing directions, and specularity of the surfaces. Butler et al. [2] evaluate this effect on a planar surface for one pose of the interfering sensor and 4 different poses of the measuring sensor. While their evaluation confirms that these factors do not significantly affect sensor accuracy nor reliability, the problem is not analyzed in detail. We consider this a highly relevant failure mode that deserves a deeper analysis.

Lemkens et al. [3] carried out a quantitative study of interference between Kinect sensors. However, they only estimate sensor reliability: standard deviation of the depth estimations. To be able to incorporate pixel failures in the analysis, they assign an arbitrary error of 5 m to missing pixel measurements, rendering the separate assessment of measurement failure and measurement accuracy impossible.

Our study considers all error interference effects independently, decreasing accuracy and reliability on the one hand and measurement failure on the other. We estimate the effect of each as a function of relative sensor placement, yielding an accurate characterization of RGB-D measurement deterioration due to interference.

### B. Solutions to Sensor Interference

Recognizing the severity of the effect of interference in RGB-D sensors, hardware modifications to RGB-D sensors were developed to eliminate or reduce the effect of sensor interference. Berger et al. [1] use a mechanical system of rotating disks with cut-outs to mechanically schedule depth sensing between multiple Kinects. Faion et al. [11] achieve the same by adding circuitry to four Kinects that can quickly turn the infrared projector on and off. Schröder et al. [12] also propose a time scheduling using LCD shutters. Such scheduling of multiple Kinects eliminates interference without degrading the RGB and depth quality at the expense of the frame rate.

Maimone and Fuchs [13] and Butler et al. [2] exploit motion blur to reduce the interference between two Kinects. They attach a rotating eccentric weight to one of the Kinects, causing it to vibrate. The small relative motion between the two Kinects causes each of them to perceive the projected infrared pattern of the other Kinect with motion blur. As each camera can perceive its own pattern without motion blur, the effect of interference is reduced significantly. However, the RGB stream of each one of the Kinects is also affected by the motion blur.

## IV. Characterization of Sensor Interference

### A. Overall Experimental Setup

We measure the degradation of the sensor signal due to interference in an RGB-D sensor, which we call the *reference sensor*, to distinguish it from the *interfering sensors*. We define the *interference region* as the area in the image of the reference sensor where the IR patterns of the interfering sensors overlap with the pattern of the reference sensor. Failures and errors also occur outside of the interference

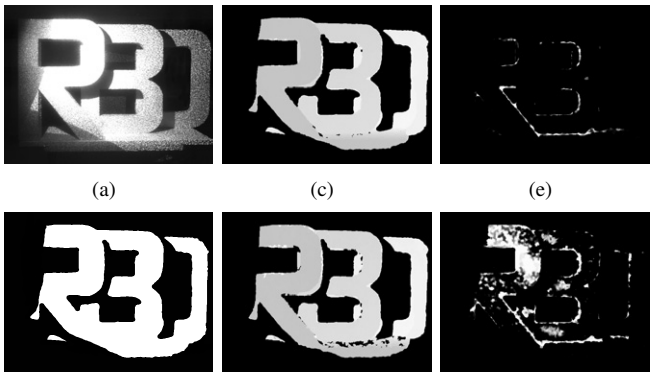

(a) (c) (e)

(b) (d) (f)

Fig. 3. Determining the effects of interference on depth measurement failure: (3(a)) IR pattern of the interfering sensor perceived by the reference sensor, (3(b)) estimated interference region, (3(c)) mean depth map in the interference region without interference (brighter is closer, depth resolution is 0.5 cm),(3(d)) mean depth map in the interference region with interference, (3(e)) probability of measurement failure in the interference region without interference (brighter is higher), (3(f)) probability of measurement failure with interference

region, due to reflections for example, but these cannot be caused by interference and should therefore be excluded from our analysis.

To determine the interference region, we activate the IR projector of the interfering sensor(s) and deactivate the IR projector of the reference sensor. Then, we collect IR images from the reference sensor. The resulting images show the parts of the scene that are *a)* affected by the interfering sensor(s) and *b)* visible to the reference sensor. By dilating and thresholding this image, we obtain the interference region (Fig. 3(a) and 3(b)).

We use two simple scenes shown in Figure 4: a Styrofoam sphere with radius 0.1 m and a set of cardboard letters (RBO) of 0.5 m height. These two targets include curved and flat, symmetric and asymmetric, highly reflective and less reflective surfaces. The background is a hanging cloth, 2 m behind the objects, parallel to the image plane of the reference sensor. Depth measurements on the background are not considered in our evaluation.

We acquired more than 260,000 depth maps at different relative poses between the reference sensor and the interfering sensor and for different target objects. We automatize the entire estimation procedure (estimation of interference region, change in the relative pose between reference and interfering sensor, and acquisition of $N = 100$ interference-free depth maps and $N$ depth maps with interference in each of the relative poses). To achieve this, we equip each sensor with a PC-controlled servo-motor that moves a lid, covering or uncovering the sensor's IR projector. The interfering sensor is mounted on the end-effector of a PUMA-560 robot ensuring fast and accurate positioning and data acquisition. We repeat all the relative poses for distances of 1.0 m, 1.5 m and 2.0 m between reference sensor and target. We consider these distances to be the most relevant for our research field, mobile manipulation and robot interaction.

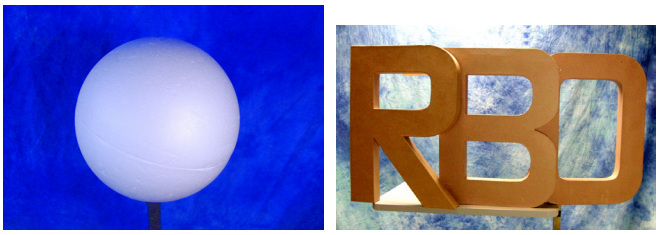

Fig. 4. Experimental scenes: a Styrofoam sphere (left, $r$ =0.1 m) and three cardboard letters (right, $h$ =0.5 m), both 2 m in front of a flat cloth background

We quantize the measurement deterioration due to interference in a particular experimental setting (scene, relative poses between reference sensor, interfering sensor, and object in the scene) by a single number. The measurement degradation due to interference, $P_I$, is the average fraction of the interference region presenting measurement failure due to interference. To present the main results of this paper, we will rely on $P_I$.

To obtain $P_I$ we first have to measure the probability of depth measurement failure without interference, $P_F$. This probability is not zero because measurement failure can be caused by some factor other than interference, for example, specularity or transparency. Then, we measure the probability of depth measurement failure when an interfering sensor(s) is active, $P_{F\cup I}$, which could be caused by interference or by something else. The probability of depth measurement failure due to interference alone, $P_I$, can then be computed as:

$$P_I = \frac{P_{F\cup I} - P_F}{1 - P_F} \tag{1}$$

Each measured probability is determined by the average fraction of the interference area over the $N$ depth maps in which no valid depth measurement was obtained under the relevant conditions (relative pose between sensors and object, interference/no interference). We obtain these required probabilities ($P_F$, $P_{F\cup I}$) by counting the number of invalid measurements in pixels of the interference area over the $N$ depth maps, $PX^{invalid}$, and dividing by the number of depth maps $N$ and the number of pixels in the interference area $PX^{IA}$:

$$P = \frac{1}{N \cdot PX^{IA}} PX^{invalid} \tag{2}$$

Based on these preliminaries, we can now describe the experiments and the implied characterization of measurement degradation. We begin by analyzing measurement failure and then continue with the evaluation of measurement accuracy and precision over all experiments.

### B. Two sensors with Intersecting Viewing Direction

*a) Experimental Setup:* We estimate measurement degradation at different relative poses of two sensors when both are oriented towards the center of the observed target. We place the reference sensor at three different distances $d$ to the target center: 1.0 m, 1.5 m and 2.0 m. At each of these distances, we measure the effect of the interference due to a

second sensor placed relative to the reference sensor and the target. The poses of the interfering sensor are chosen to lie on spheres of varying radii centered at the target. We sample interfering sensor poses at five radii: $d$-50 cm, $d$-25 cm, $d$, $d$+25 cm and $d$+50 cm. Azimuth and elevation of the sample positions vary between $\pm 30^\circ$ in azimuth and $-20^\circ$ to $30^\circ$ in elevation, in steps of approximately $10^\circ$ relative to the reference sensor. This amounts to 434 valid relative poses for the Styrofoam sphere target and 425 relative poses for the cardboard letters target. Figure 5(a) illustrates the setup with the target object and the three distances between the reference sensor and the target.

*b) Results and Discussion:* Figures 5(b) and 5(c) depict the average fraction of the interference region presenting measurement failure due to interference, $P_I$, at each sampled interfering sensor pose for two targets at one distance between reference sensor and target. Average probability values are color coded and interpolated between the sample points. Intuition is confirmed as the average fraction of the interference region presenting measurement failure increases inversely proportionally to the distance between sensors and target. Figure 5(b) shows the worst observed case: reference sensor distanced 1 m of the Styrofoam sphere. In this case, on the front layer of the analysis (interfering sensor at 0.5 m of the target, different azimuth and elevation values) nearly the entire (95%) depth information is lost due to interference.

Figure 5(c) shows a less extreme case where the distance between the reference sensor and the object is 1.5 m. Although the maximum in the average fraction of the interference region presenting measurement failure differs (15% when the interfering sensor is placed 1 m from the cardboard letters), the overall structure is the same as before. The distance between interfering sensor and target is clearly the most significant parameter that determines the average fraction of the interference region presenting measurement failure.

In this setting, the crucial factor for measurement deterioration is the distance of the sensors to the target. Figure 5 shows that the variation with the distance is stronger than the variation in orientation (layers of the "onion" are mostly of identical color). When the sensors are very close to the target, their overlapped IR patterns saturate the IR camera and failures are the result. Figure 7 illustrates the worst case, in which $P_I$ reaches values of 0.95. The IR image shows how the IR pattern of the interfering sensor saturates the object surface.

A detailed analysis of the data is shown in Figure 6. For the two target objects, $P_I$ is averaged for each of the spheres and plotted as a function of their radii (distance to target). The graph shows how the effect of interference increases with proximity to target. The strength of the effect varies with surface characteristics. This data implies that both sensors should be at a distance of at least 1 m from the target. This limits the effect of interference to 10–20% of the interference region. If both sensors are at a distance of at least 1.5 m from the target, the effect of the interference is limited to 5–8% of the interference region. We test this safety margins for sensors with intersecting viewing directions in Section VI on an RGB-D-based application.

### C. Two sensors with Parallel Viewing Direction

*a) Experimental Setup:* We now explore the effect of interference for parallel viewing directions. Figure 8(a) illustrates the setup with the target object and the three distances to the reference sensor. Measurements are obtained by displacing the interfering sensor within a 3-dimensional Cartesian grid relative to the reference sensor. The grid is composed of nine planes perpendicular to the viewing direction of both cameras, with a distance of 0.1 m between them. Each plane contains 20 measuring sampling points, spaced 0.1 m in both dimensions, for a total of 180 possible relative poses.

*b) Results and Discussion:* The results of this experiment are consistent with those from the previous experiment: the most relevant parameter for the interference is the distance between sensors and target. When the interfering sensor is significantly closer than the reference sensor the IR pattern of the latter is overpowered by the IR interfering pattern and the probability of disappearing pixels rises up to 41% (Styrofoam sphere).

Figure 9 shows degradation of the measurements as a function of the proximity of sensors to target. For the two target objects, $P_I$ is averaged at each distance of the interfering sensor to the target and plotted as a function of this distance. The graph shows that the effect of interference increases with proximity to the target. However, the degradation is lower than in the first scenario. This is explained by the IR pattern being brighter in the center of the projected pattern.

This second experiment confirms that the safe area begins approximately at a distance of 1.5 m from sensed surfaces. If all sensors are at least at this safety distance, the degradation caused by the interference remains under 10%. If one sensor gets closer than this safety threshold, the perceived depth by any other sensor will rapidly decrease. We test this safety margins for sensors with parallel viewing directions in Section VI on an RGB-D-based application.

### D. Two Sensors with Opposite Viewing Directions

*a) Experimental Setup:* We now analyze the interference between two structured light sensors facing each other and thus projecting their IR light directly on the IR camera of the other sensor. The interfering sensor is placed behind a large non-reflecting paper screen with only the IR projector peeking through a hole towards the scene. The reference sensor is positioned in front of the screen facing the projector at the the same height (1 m) and at four different distances: 1.0 m, 1.5 m, 2.0 m and 2.5 m (Fig. 10(a)).

Three sets of $N = 100$ measurements are taken at different distances between camera and screen (and thus interfering sensor): one reference set of $N$ depth images with deactivated interfering sensor, one set of $N$ degraded depth images in which one of the infrared speckle emitted by the interfering sensor directly shines into the infrared camera of the reference sensor, and one set of $N$ degraded depth images in

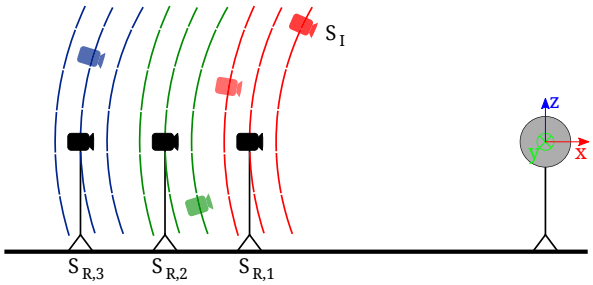


(a) Experimental setup for two sensors with intersecting viewing direction: the reference sensor, $S_R$, is placed at three different distances to the target, shown in gray, and the interfering sensor $S_I$ is placed on concentric spheres around the target, pointing towards the sphere's center

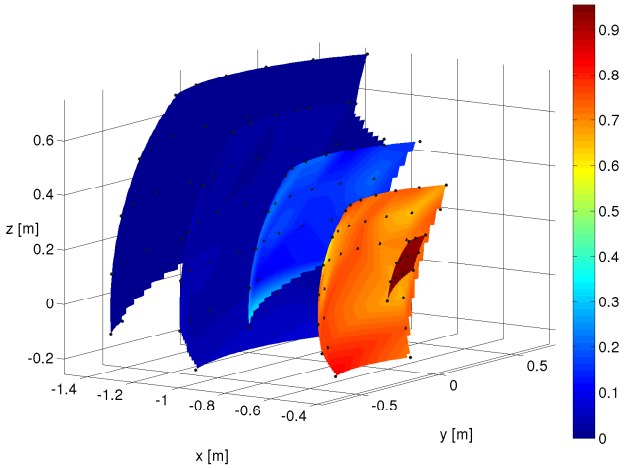


(b) Average fraction of the interference region presenting measurement failure, $P_I$, at distance of 1 m from the reference sensor to the Styrofoam sphere and several interfering sensor poses

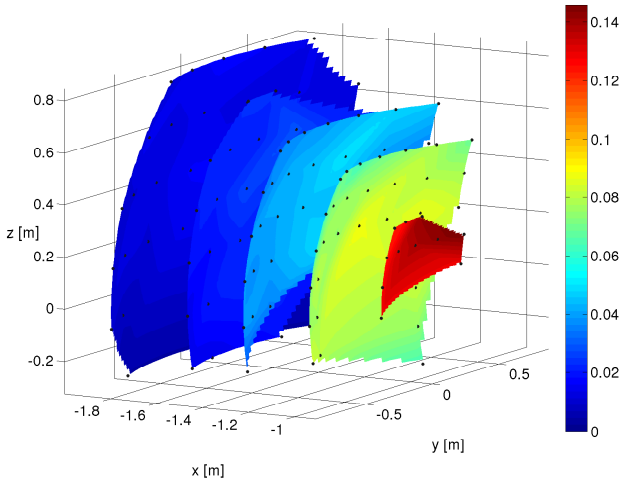


(c) Average fraction of the interference region presenting measurement failure, $P_I$, at distance of 1.5 m from the reference sensor to the cardboard letters and several interfering sensor poses

Fig. 5. Intersecting viewing directions—experimental setup and results: the scale of the results is adapted to the range of values, please consider the legend; the origin of coordinates is placed at the center of the target

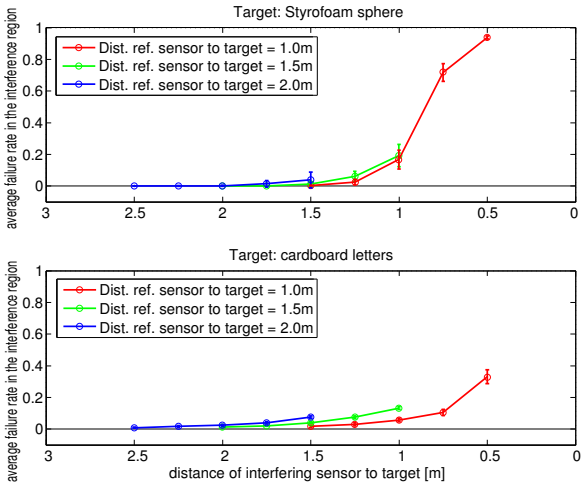


Fig. 6. Intersecting viewing directions—Average fraction of the interference region presenting measurement failure as a function of proximity of the interfering sensor to the target

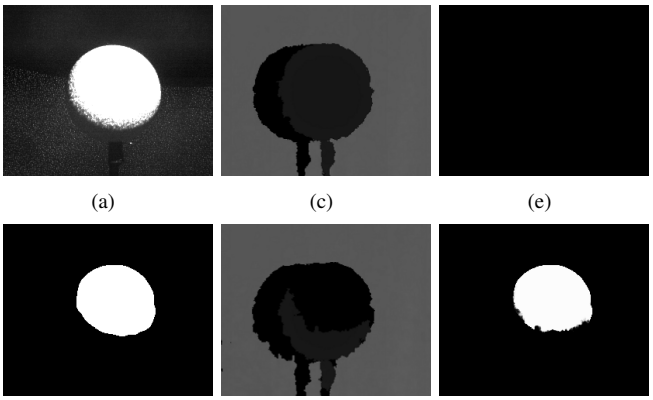

(a) (c) (e)

(b) (d) (f)

Fig. 7. Worst effect of interference when two sensors are pointing at the same target (reference sensor 1 m from the target, interfering sensor 0.5 m): (7(a)) IR pattern from the interfering sensor perceived by the reference sensor, (7(b)) resulting interfering region, (7(c)) resulting depth map without interference, (7(d)) resulting depth map with interference, (7(e)) probability of measurement failure in pixels of the interference region without interference (brighter is higher), (7(f)) probability of measurement failure in pixels of the interference region when activating the interfering sensor

which the emitted interfering IR pattern does not directly shine into the IR camera. We used a video camera with IR filter to adjust the pose of the interfering sensor so that we can obtain measurements in the two interfering scenarios.

*b) Results and Discussion:* Our measurements indicate that under unfavorable conditions up to 9% of the pixels in the interference region will fail to register depth measurements. However, the effect of interference from opposing viewing directions is much lower that the effect measured in our first two experiments. Measurement deterioration is pronounced at short distances (less than 1.0 m) and quickly decays with distance; at 2.5 m it is less than 1 %. This can be explained with the quadratic decay in intensity of the IR projection.

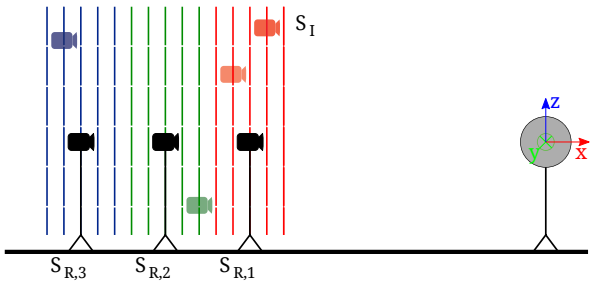


(a) Experimental setup for two sensors with parallel viewing directions: the reference sensor $S_R$ is placed at three distances to the object and the interfering sensor $S_I$ (color) is placed in various relative locations with a parallel viewing direction

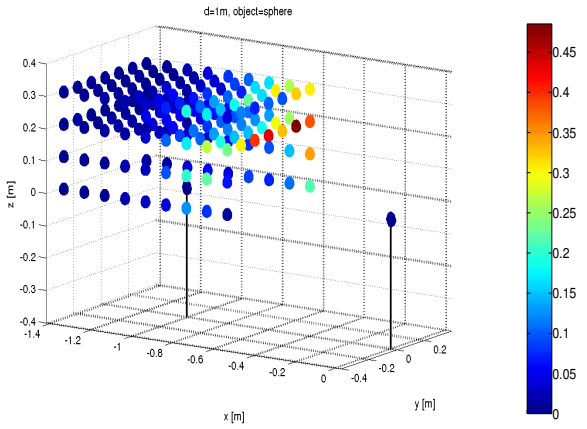


(b) Average fraction of the interference region presenting measurement failure, $P_I$, at distance of 1 m from the reference sensor to the Styrofoam sphere and several interfering sensor poses

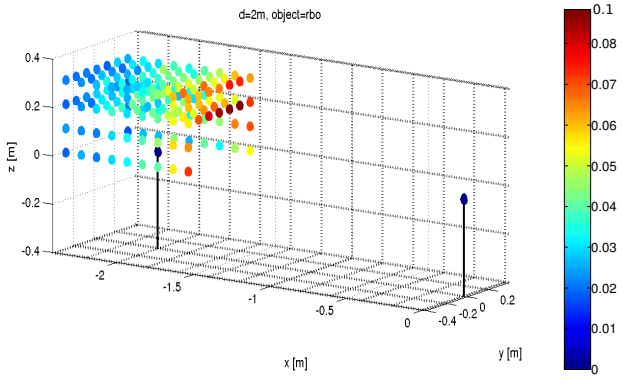


(c) Average fraction of the interference region presenting measurement failure, $P_I$, at distance of 2 m from the reference sensor to the cardboard letters and several interfering sensor poses

Fig. 8. Parallel viewing directions—experimental setup and results: the scale of the results is adapted to the range of values, please consider the legend; the origin of coordinates is placed at the center of the target

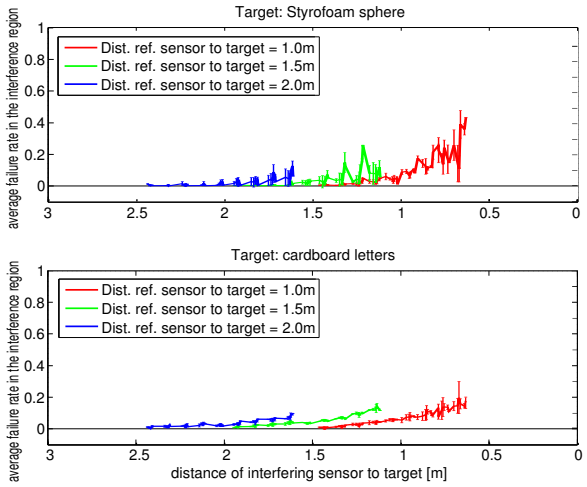


Fig. 9. Parallel viewing directions—Average fraction of the interference region presenting measurement failure as a function of proximity of the interfering sensor to the target

### *E. Effect of Interference on Accuracy and Precision*

*a) Experimental Setup:* We can use all of the measurements taken above to assess the degradation of sensor accuracy (error between the mean depth value and the ground truth value at each pixel) and precision (standard deviation of the depth values at each pixel) due to interference between two sensors. Accuracy and reliability are computed using only valid depth measurements. Instead of measuring the absolute accuracy, which requires a ground truth value for each pixel measurement, we measure the degradation of the accuracy as the difference in the mean depth pixel value obtained from the $N$ depth maps without interference and the $N$ depth maps with interference. The depth resolution of the sensor depends on the distance: 2 mm at 1 m, 6 mm at 1.5 m, 1 cm at 2 m [14]. These are upper boundaries for the accuracy of the sensor.

*b) Results and Discussion:* The degradation on accuracy and reliability due to interference is negligible compared to the measurement failures observed in previous experiments. The accuracy of most pixels in the interference region (more than 99% of the pixels) differs less than 1 cm between measurements with and without interference. For less than 1% of the pixels the accuracy decreases more than 1 cm. This can be observed in Fig. 3(c) and Fig. 3(d) showing that the mean depth measurements for pixels in the interference region are mostly the same in both scenarios, even on the areas where the probability of measurement failure due to interference is high (Fig. 3(f)).

We estimate the reliability as the standard deviation of the depth measurements (only valid ones) in the interference region around the mean depth value. The reliability of these pixels in the interference scenario remains around 0.01 m, similar to the reliability of these pixels without interference. Only for the same 1% of the pixels with degraded accuracy, the reliability also degrades to almost 0.05 m. These results are consistent with most of the previous interference studies

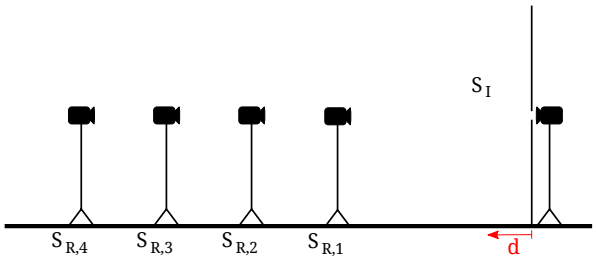


(a) Experimental setup for two sensors with opposite viewing direction: the reference sensor $S_R$ and the interfering sensor $S_I$ face each other at different distances

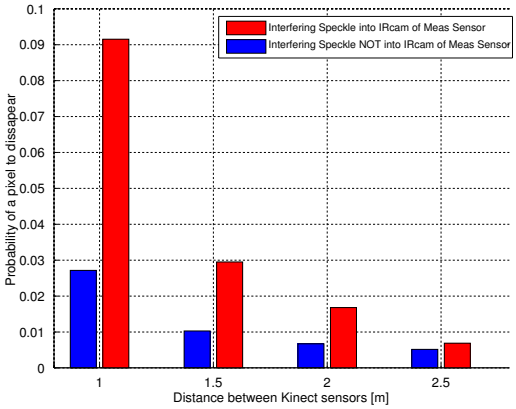


(b) Interference due to direct opposition of two sensors: the maximum measurement deterioration is observed when one speckle of the interfering pattern points directly on the IR camera of the reference sensor

Fig. 10. Opposite viewing directions—experimental setup and results

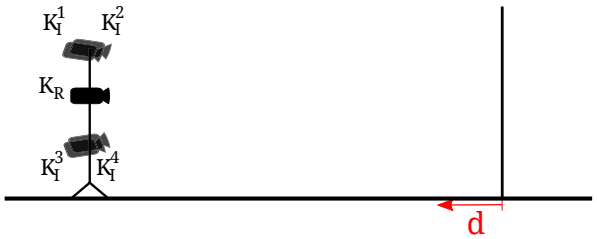


Fig. 11. Experimental setup for several sensors: the reference sensor $S_R$ is surrounded by four interfering sensors $S_I^i$

(see Section III).

### F. More Than One Interfering Sensor

*a) Experimental Setup:* We measure the degradation of the depth signal in the reference sensor when 1, 2, 3, or 4 sensors are interfering with it (with intersecting viewing directions). All sensors are placed 2 m away from a planar, non-reflecting paper screen, with their viewing directions intersecting at a point on the surface. The reference sensor is placed in the center of a 1.5 $m^2$ square, parallel to the image plane and the observed surface. The interfering sensors are placed at the corners of that square (Figure 11).

*b) Results and Discussion:* The average fraction of the interference region of the five IR patterns presenting measurement failure grows from 0% when no other sensor is interfering to almost 25% of the image when four sensors are interfering. This is significantly higher than four times the interference caused by one sensor, and thus, the interference is not linear with the number of sensors. The degradation of the depth signal is substantial and should be considered in environments with more than two structured light sensors. The safety margins inferred from the experiments of two sensors cannot be used in scenarios with more than two sensors. We recommend an analysis of the interference degradation for each specific application that requires more than two sensors.

## V. Recommendations

Based on the experimental results, we provide a set of recommendations for the use of multiple RGB-D sensors in the same workspace. The most important factors affecting measurement quality are: reflectivity of the target surface, sensors' viewing direction, distance between sensors and target, and number of sensors. For scenarios with two sensors, a distance of at least 1.5 m between sensors and target ensures that less than 10 % of the depth measurements in the interference region will fail. This applies for intersecting and parallel viewing directions, for reflecting and non-reflecting surfaces. For applications in which sensors may be closer to the target than 1.5 m, the degradation of the measurements increases with the reflectivity of the surface and is higher for intersecting viewing directions. When more than two sensors share a workspace, the interference degrades the depth measurements significantly even if the sensors are more than 1.5 m away from the observed objects. When more than two sensors are involved, an analysis comparable to the one presented here becomes difficult; we recommend an analysis tailored to the specific setup and application.

## VI. Interference in an RGB-D-Based Application

We demonstrate that an accurate understanding of measurement deterioration in RGB-D sensors due to IR interference can be highly relevant for applications using such sensors. We therefore apply the insights gained from our experiments to an application using RGB-D data: the iterative closest point (ICP) based solution for simultaneous localization and mapping (SLAM) from ETH Zurich[1]. This algorithm uses a down-sampled RGB-D stream to build a map of the environment and simultaneously tracks the camera on the map using ICP. We placed the reference sensor at three different distances (1.0 m, 1.5 m and 2.0 m) of a group of objects with various reflection properties. We built a map of the scene using the SLAM package and move the sensor to verify that the ICP-based SLAM localization works correctly. Then we place a second sensor (interfering sensor) at several distances to the target (from 0.5 m to 2.0 m in steps of 0.25 m) and test the ICP-based SLAM localization again. We examine the case when the two sensors have parallel and aligned viewing directions. We observe two error cases in the ICP-based localization caused by the interference: either

[1]Available as open package for the Robotic Operating System (ROS) at `http://wiki.ros.org/ethzasl_icp_mapping`

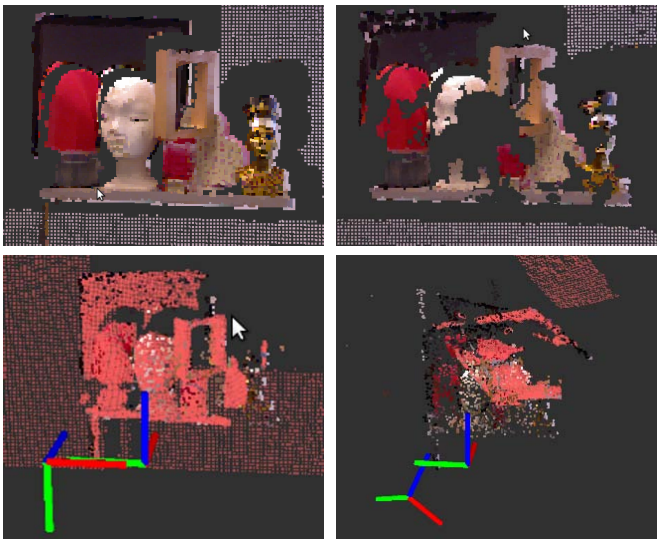

Fig. 12. Effect of sensor interference on a RGB-D based application. An ICP-based SLAM algorithm uses the RGB-D stream to build a map of an scene. Then, it continuously localizes the sensor in the map. When there is no interference the algorithm converges (left column). If a second sensor (interfering sensor) is active within the margins, the algorithm converges to a wrong pose (right column).

TABLE I

EFFECT OF INTERFERENCE IN AN RGB-D-BASED APPLICATION

| $S_\times$ | distance of $S_R$ to object | | | | | |
|---|---|---|---|---|---|---|
| | 1.0 m | | 1.5 m | | 2.0 m | |
| | $\parallel$ | $\perp$ | $\parallel$ | $\perp$ | $\parallel$ | $\perp$ |
| 0.5 | ××× | ××× | ××× | ××✓ | × ✓✓ | ××✓ |
| 0.75 | ××× | ××× | ××× | ××✓ | ✓✓✓ | ✓✓✓ |
| 1.0 | ××✓ | ×✓✓ | ××✓ | ×✓✓ | ✓✓✓ | ✓✓✓ |
| 1.25 | ××✓ | ✓✓✓ | ×✓✓ | ✓✓✓ | ✓✓✓ | ✓✓✓ |
| 1.5 | ✓✓✓ | ✓✓✓ | ✓✓✓ | ✓✓✓ | ✓✓✓ | ✓✓✓ |
| 1.75 | ✓✓✓ | ✓✓✓ | ✓✓✓ | ✓✓✓ | ✓✓✓ | ✓✓✓ |
| 2.0 | ✓✓✓ | ✓✓✓ | ✓✓✓ | ✓✓✓ | ✓✓✓ | ✓✓✓ |

Interference degradation of an RGB-D-based SLAM algorithm: crosses indicate failure, checkmarks indicate stable localization; experiments varied the distances of the interfering sensor $S_I$ and the reference sensor $S_R$ to the object; measurements were taken for parallel viewing directions ($\parallel$) and for intersecting viewing directions ($\perp$)

the algorithm fails to converge and returns a camera pose out of bounds (as determined by the algorithm itself), or the algorithm converges to a wrong localization (observable through visualization of the alignment of the current point cloud to the map, see Fig. 12).

Table I summarized the failures of the ICP-based SLAM algorithm. The results support the safety margin we obtained from our analysis: if both sensors are at a distance of at leat 1.5 m from the object, the degradation due to interference remains under 10% and the RGB-D-based SLAM successfully locates the reference sensor by aligning the current point cloud to the map. The degradation of the signal increases inversely proportional to the distance of sensors to the target. If one sensor is closer than the safety margin, the SLAM application becomes unreliable and fails.

These results demonstrate the importance of considering the effects of measurement deterioration due to sensor interference in real-world robotic applications.

## VII. CONCLUSION

We presented the first in-depth analysis of measurement deterioration in RGB-D sensor due to interference of projected IR patterns. Our analysis revealed that depth measurement failures are frequently the result of such interference. In some cases, up to 95% of depth measurements in the interference region fail. We examined the effect of interference in extensive experiments, considering several scenarios: two sensors looking at the same object, two sensors looking into the same direction, two sensors looking at each other and more than two sensors. The fraction of the interference region presenting measurement failure depends strongly on the distance between sensors and observed object. Surprisingly, sensor interference has little effect on measurement accuracy and precision, it only causes measurement failure. This implies that the effects of sensor interference can be detected directly in the measurement data: sensor failure at a particular pixel will result in an invalid depth measurement. Applications can therefore detect measurement failure and react appropriately. We demonstrated in a real-world SLAM application that the insights derived from our experiments help avoid failures of the application due to measurement deterioration.

## REFERENCES


[1] K. Berger, K. Ruhl, C. Brümmer, Y. Schröder, A. Scholz, and M. Magnor, "Markerless motion capture using multiple color-depth sensors," in *Proc. Vision, Modeling and Visualization (VMV)*, 2011.

[2] D. A. Butler, S. Izadi, O. Hilliges, D. Molyneaux, S. Hodges, and D. Kim, "Shake'n'sense: Reducing interference for overlapping structured light depth cameras," in *Proc. of SIGCHI*, 2012, pp. 1933–1936.

[3] W. Lemkens, P. Kaur, K. Buys, P. Slaets, T. Tuytelaars, and J. D. Schutter, "Multi rgb-d camera setup for generating large 3d point clouds," in *International Conference on Intelligent Robots and Systems*, 2013.

[4] M. Minou, T. Kanade, and T. Sakai, "A method of time-coded parallel planes of light for depth measurement," *Trans. Institute of Electronics and Communication Engineers of Japan*, vol. 64, pp. 521–528, 1981.

[5] M. Proesmans, L. Van Gool, and F. Defoort, "Reading between the lines-a method for extracting dynamic 3d with texture," in *Conference on Computer Vision*, 1998, pp. 1081–1086.

[6] G. Sansoni, S. Corini, S. Lazzari, R. Rodella, and F. Docchio, "Three-dimensional imaging based on gray-code light projection: characterization of the measuring algorithm and development of a measuring system for industrial applications," *Applied Optics*, vol. 36, 1997.

[7] A. Shpunt and Z. Zalevsky, "Three-dimensional sensing using speckle patterns," Primesense LTD patent, US 2009/0096783 A1, 2009.

[8] B. Freedman, A. Shpunt, M. Machline, and Y. Arieli, "Depth mapping using projected patterns," Primesense LTD patent,US 2010/0118123 A1, 2010.

[9] M. Andersen, "Kinect depth sensor: Evaluation for computer vision applications," Aarhus University, Tech. Rep. ECE-TR-6, 2012.

[10] M. Viager, "Analysis of kinect for mobile robots," DTU Electrical Engineering Technical University of Denmark, Report, 2011.

[11] F. Faion, S. Friedberger, A. Zea, and U. D. Hanebeck, "Intelligent sensor-scheduling for multi-kinect-tracking," in *International Conference on Intelligent Robots and Systems*, 2012, pp. 3993–3999.

[12] Y. Schröder, A. Scholz, K. Berger, K. Ruhl, S. Guthe, and M. Magnor, "Multiple kinect studies," ICG, Tech. Rep. 09-15, Oct. 2011.

[13] A. Maimone and H. Fuchs, "Reducing interference between multiple structured light depth sensors using motion," in *IEEE Virtual Reality Conference*, 2012, pp. 51–54.

[14] K. Khoshelham and S. O. Elberink, "Accuracy and resolution of kinect depth data for indoor mapping applications," *Sensors*, vol. 12, no. 2, pp. 1437–1454, 2012.